DOI: 10.21062/mft.2024.005 http://www.journalmt.com

Motion Planning and Simulation of Multifunctional Over-the-tube Pipe Climbing Robot

Li Dong (0009-0007-8270-1802)[1], Tongchao Xing (0009-0009-4086-2514)[2], Yi Zheng (0000-0002-7853-8279)[1,3*]
[1]Institute of Intelligent Manufacturing, Qingdao Huanghai University, Qingdao, Shandong, 266427, China
[2]Offshore Oil Engineering Qingdao Co., Ltd., Qingdao, Shandong, 266400, China
[3*]School of Mechanical and Automotive Engineering, Qingdao University of Technology, Qingdao, 266520, China
*Corresponding Author: Email:fw.2004@163.com

Due to the complexity of the current industrial pipeline layout, in order to improve the efficiency of pipeline inspection and maintenance, a multi-functional obstacle-surmounting pipe-crawling robot was designed to address the issues of varying pipe diameters and positions. The movement pattern of the crawling robot was studied, the variation of the clamping force of the clamping mechanism during the climbing process was analyzed, and the mapping relationship between various parameters was obtained as the basis for later kinematic simulation. The design of inverted V, positive V and other drive combinations and the planning of multi-functional obstacle-surmounting actions were conducted to verify the rationality of the structural design and the stability of the motion process of the multi-functional obstacle-surmounting pipe-crawling robot. Results showed that the multi-functional obstacle-surmounting pipe-crawling robot can achieve the expected crawling speed of 0.3m/s when moving on a horizontal pipeline, and the motion process is stable. When moving on a vertical pipeline, from the speed and displacement curve of the robot on the x, y, and z axes, it can be seen that the speed and displacement of the pipe-crawling robot are steadily increasing without any left or right swing, indicating that the clamping mechanism works well and the structural design is reasonable.

Keywords: External crawling pipe robot; Multi-functional obstacle crossing; Motion planning; Motion simulation

1 Introduction

On January 19, 2023, the Ministry of Industry and Information Technology of China released the "Robot +" Application Action Implementation Plan, proposing ten major application scenarios. The plan states that by 2025, the density of manufacturing robots will double that of 2020, and the depth and breadth of application in service robots and special robots industries will be significantly improved, enhancing the ability of robots to promote high-quality economic and social development. With a focus on the ten major application areas, breakthroughs will be made in more than 100 new robot application technologies and solutions, and over 200 typical robot application scenarios with a high level of technical expertise, innovative application modes, and significant application effects will be promoted to create a group of benchmark enterprises for "Robot + " applications. The ten major application areas include the manufacturing industry, agriculture, construction, energy, trade and logistics in the economic field, as well as medical health, elderly care services, education, business community services, safety emergency, and extreme environment applications in the field of social people's livelihood.

Currently, pipeline inspection and maintenance work is mostly repetitive and has high labor intensity with low work efficiency and extremely high danger. Additionally, many industrial pipelines transport fluids that are high-temperature, high-pressure, toxic, and radioactive, which further increases the danger of the work. Therefore, there is an urgent need to develop a multi-functional pipeline climbing robot with obstacle-crossing capabilities to replace manual inspection and maintenance.

2 Mechanical Structural Design of Pipe-Climbing Robot

2.1 Overall Structural Design

To address the above issues, this project has designed a multi-functional pipe-climbing robot with obstacle-crossing capabilities. The overall structure of the robot is articulated and divided into front and rear sections, with each section designed with gripping and supporting mechanisms. A flipping mechanism is designed between the front and rear sections. The final established structure model is shown in Fig. 1.

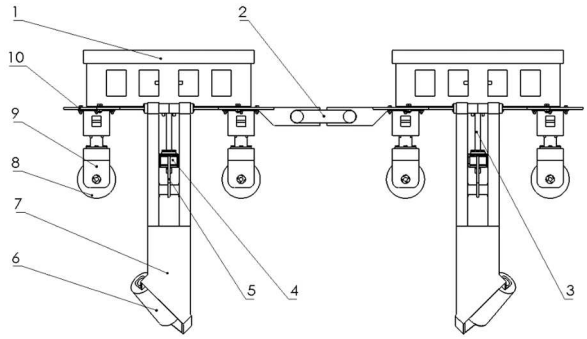

Fig. 1 *Structure diagram of the pipe-climbing robot outside the pipe*

Where:
1…Load-bearing frame;
2…Flipping mechanism;
3…Electric screw;
4…Supporting frame;
5…Connecting rod;
6…Steering drive wheel;
7…Hugging arm;
8…Walking wheel;
9…Walking wheel connecting frame;
10-Vehicle frame.

2.2 Clamping mechanism

The Clamping mechanism consists of an electric screw, a spreading frame, a connecting rod, a holding arm, and a steering driving wheel and motor. When the holding action starts, the electric screw first starts and drives the spreading frame that is fixedly connected to the electric screw to move up and down. The two connecting rods on both sides that are hinged to the spreading frame rotate. The holding arm hinged to the connecting rod can hold the pipeline through the steering driving wheel. The schematic diagram of the holding process is shown in Figure 2, from Figure 2 (a) to Figure 2 (b) is the process of tightening the holding arm.

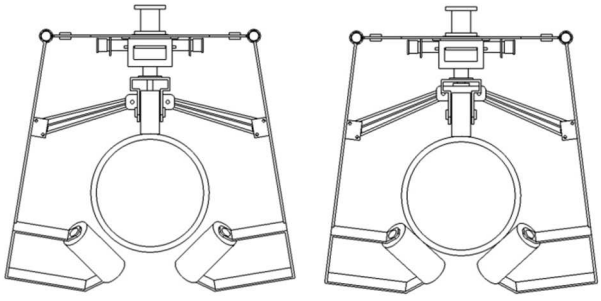

Fig. 2 *Working process of hugging arm*

2.3 Flip Mechanism

The flip mechanism is controlled by a servo, which rotates a corresponding angle to drive the flip of the front and rear chassis. The stability of the flip mechanism determines whether the robot can smoothly cross obstacles, and the selection of servo torque is critical for the flip mechanism to correctly receive obstacle-crossing instructions. The design of servo parameters will be explained in detail in Chapter 5, and the schematic diagram of flipping action is shown in Figure 3.

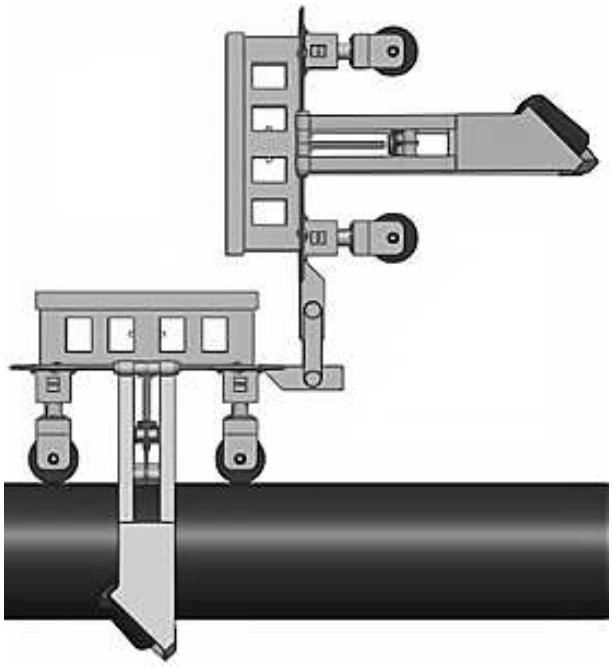

Fig. 3 *Schematic diagram of overturning action*

3 Analysis of Motion Characteristics of Pipe Crawling Robot outside Pipe

According to the simplified mathematical model of the three-dimensional model of the Pipe Crawling Robot outside Pipe shown in Figure 4, the expressions for the link angle, link angular velocity, and link angular acceleration can be obtained when the link length, slider offset e, and slider velocity are known.

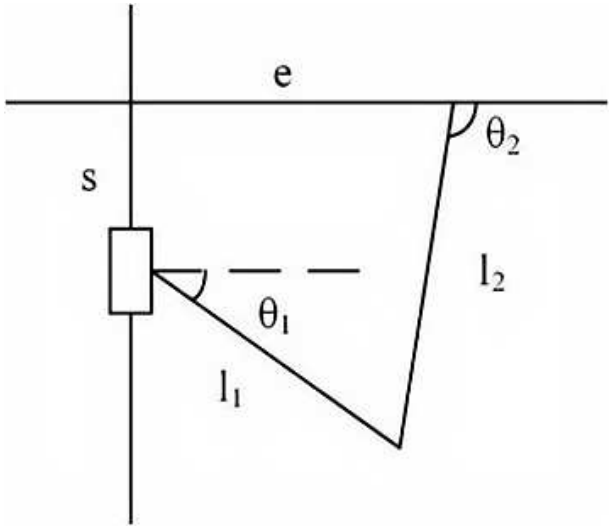

Fig. 4 *schematic diagram of mathematical model*

Establish the equations of X direction and Y direction.

$$\text{X direction:} \quad l_1 \cos\theta_1 - l_2 \cos\theta_2 = e \tag{1}$$

$$\text{Y direction:} \quad l_2 \sin\theta_2 - l_1 \sin\theta_1 = s \tag{2}$$

The slider displacement can be obtained from equations (1) and (2).

$$s = l_1 \sin\theta_1 - \sqrt{l_2^2 - (l_1 \cos\theta_1 - e)^2} - l_1 \sin\theta_1 \tag{3}$$

The slider speed can be obtained by taking the derivative of time t from Equation (3).

$$v = \frac{l_1 \sin\theta_1 (l_1 \cos\theta_1 - e)}{\sqrt{l_2^2 - (l_1 \cos\theta_1 - e)^2}} - l_1 \cos\theta_1 \tag{4}$$

The slider acceleration can be obtained by deriving the time t from Equation (4).

$$a = l_1 \sin\theta_1 + \frac{l_1^2 \cos 2\theta_1 - e l_1 \cos\theta_1}{\sqrt{l_2^2 - (l_1 \cos\theta_1 - e)^2}} - \frac{l_1^2 \sin^2\theta_1 (l_1 \cos\theta_1 - e)^2}{\left[l_2^2 - (l_1 \cos\theta_1 - e)^2\right]^{\frac{3}{2}}} \tag{5}$$

The connecting rod angle θ_2 can be obtained from equations (1), (2) and (3).

$$\theta_2 = \arctan \frac{\sqrt{l_2^2 - (l_1 \cos\theta_1 - e)^2}}{l_1 \cos\theta_1 - e} \tag{6}$$

The angular velocity ω_2 of the connecting rod can be obtained by deriving the time t from equation (6).

$$\omega_2 = \frac{(l_1 \cos\theta_1 - e)^2}{(l_1 \cos\theta_1 - e)^2 + \sqrt{l_2^2 - (l_1 \cos\theta_1 - e)^2}} \tag{7}$$

The angular acceleration of the connecting rod can be obtained by deriving the time t from Equation (7).

$$a_2 = \frac{2 l_1 \sin\theta_1 (l_1 \cos\theta_1 - e)}{(l_1 \cos\theta_1 - e)^2 + \sqrt{l_2^2 - (l_1 \cos\theta_1 - e)^2}} - \frac{l_1 \sin\theta_1 (l_1 \cos\theta_1 - e)^3 (1 - 2\sqrt{l_2^2 - (l_1 \cos\theta_1 - e)^2})}{\sqrt{l_2^2 - (l_1 \cos\theta_1 - e)^2}\left[(l_1 \cos\theta_1 - e)^2 + \sqrt{l_2^2 - (l_1 \cos\theta_1 - e)^2}\right]} \tag{8}$$

4 Multi-functional obstacle-crossing motion planning

4.1 Mobility Motion Planning

The basic climbing actions of the pipe-climbing robot inside the pipe are forward and backward movements along the pipeline. However, the forward and backward movements of the pipe-climbing robot outside the pipe are achieved by the coordinated rotation of the two steering driving wheels on both sides. During forward movement, the outer pipe-climbing robot starts from a stationary position and clamps the pipe with the clamping mechanism. The left-side steering driving wheel of the front frame rotates clockwise under the drive of the stepper motor, while the right-side steering driving wheel of the front frame rotates counterclockwise under the drive of the stepper motor. The steering driving wheels on both sides of the rear frame work in the same way to achieve forward movement. The motion during backward movement is the same as that during forward movement, except that the rotation direction of the steering driving wheels is different. The left-side steering driving wheel of the front frame rotates counterclockwise under the drive of the stepper motor, while the right-side steering driving wheel of the front frame rotates clockwise under the drive of the stepper motor. The steering driving wheels on both sides of the rear frame work in the same way to achieve backward movement. As shown in Figure 5, Figure 5a is a schematic diagram of the rotation direction of the forward steering driving wheel, and Figure 5b is a schematic diagram of the rotation direction of the backward steering driving wheel.

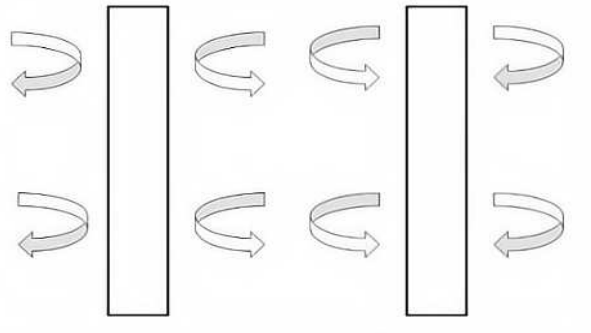

Fig. 5 *Schematic diagram of forward and backward movement*

4.2 Rotation motion planning

The rotation motion of the pipe-climbing robot outside the pipe can be divided into rotating in place around the pipeline and spiraling forward around the pipeline. When rotating in place around the pipeline, the clamping mechanism clamps the pipeline, the left and right steering drive wheels of the front frame rotate clockwise, and the left and right steering drive wheels of the rear frame also rotate clockwise, realizing the pipe-climbing robot's rotation to the right around the pipeline. For turning left, all steering drive wheels need to rotate counterclockwise. As shown in Figure 6, Figure 6a illustrates the direction of rotation of the steering drive wheel when rotating to the right in place, and Figure 6b illustrates the direction of rotation of the steering drive wheel when rotating to the left in place.

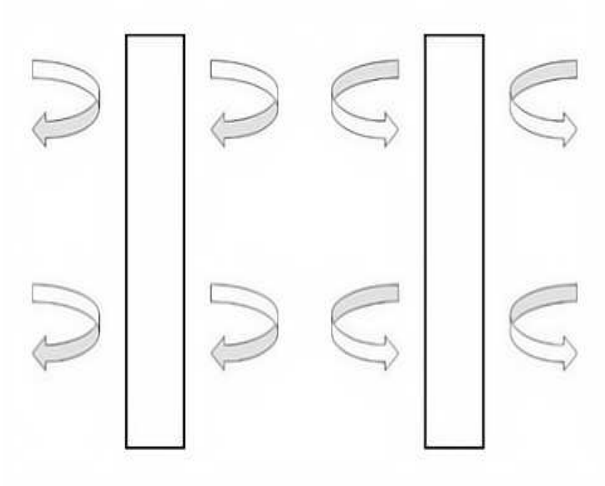

Fig. 6 *Schematic diagram of in-situ rotation*

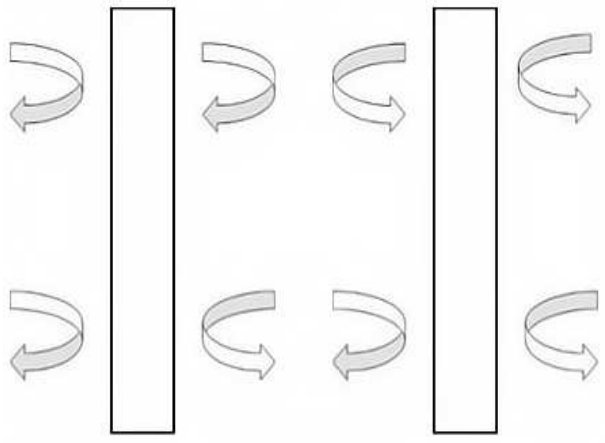

Fig. 7 *Schematic diagram of spiral advance*

When the spiral is moving forward or backward along the pipeline, simply reverse the direction of the driving wheel that was originally rotating in place. When the spiral moves forward in a right-handed spiral around the pipeline, the left and right steering driven wheels of the front chassis rotate clockwise, the right steering driven wheel of the rear chassis rotates counterclockwise, and the left steering driven wheel of the rear chassis rotates clockwise. When the spiral moves forward in a left-handed spiral around the pipeline, the left and right steering driven wheels of the front chassis rotate counterclockwise, the left steering driven wheel of the rear chassis rotates clockwise, and the right steering driven wheel of the rear chassis rotates counterclockwise. As shown in Figure 7, Figure 7a shows the schematic diagram of rotating to the right, and Figure 7b shows the schematic diagram of rotating to the left.

4.3 Obstacle-Crossing Action Planning

The obstacle-crossing actions of the crawling robot outside the pipe include crossing obstacles on the outer surface of the pipeline and crossing the cross joints within the pipeline, as shown in Figure 8. Cross joints are an important issue in pipeline obstacle-crossing research, which requires the crawling robot outside the pipe to have obstacle-crossing capabilities and adaptability to changes in pipe diameter. There are several methods for crossing cross joints, including (a) cross joints perpendicular to the ground- As shown in Figure 9, which is a schematic diagram of a cross joint perpendicular to the ground. From A to C, the robot first travels horizontally in the pipe, then lifts the front part until the rolling wheels touch the pipe, clamps the clamping mechanism, and then travels vertically on the pipe. When it reaches a position that can accommodate the rear part of the frame, the rear part of the robot falls. From B to C, the robot rotates in place from B to position A, and then moves from A to C. The same is true for A to D and B to D, allowing the robot to rotate in place.

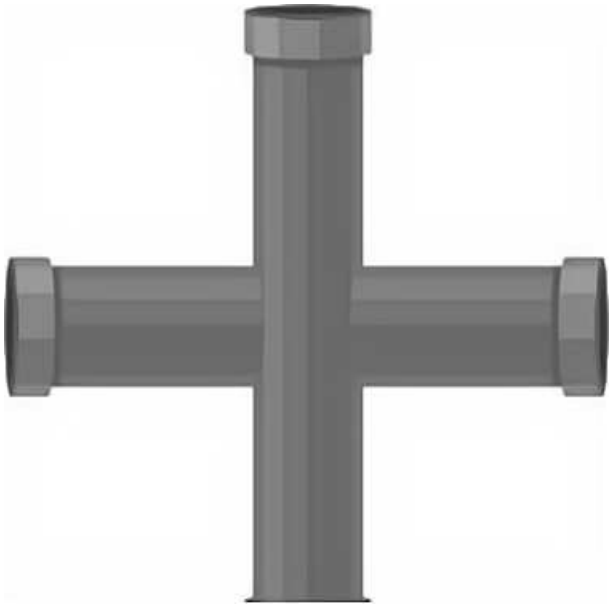

Fig. 8 *Cross-shaped pipeline*

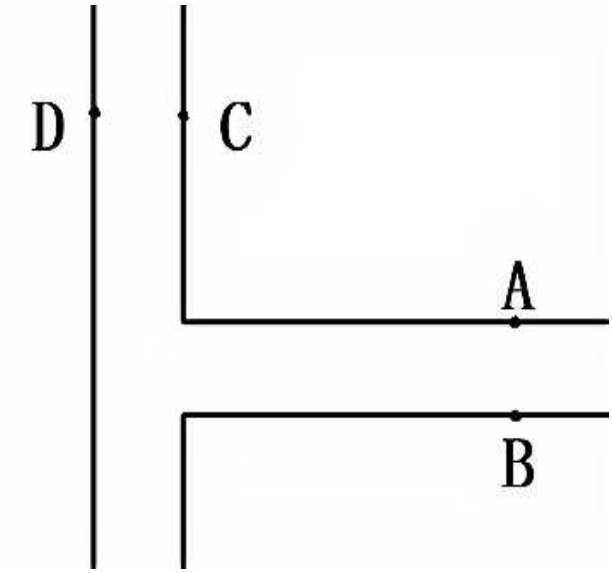

Fig. 9 *schematic diagram of cross-shaped pipeline perpendicular to the ground*

Crossbar parallel to the ground As shown in Figure 10, this is a schematic diagram of the crossbar parallel to the ground. From A to B, it can be traveled straight through the horizontal pipeline, and then the front frame is lifted to move forward. After the front frame has crossed the crossbar, it falls down, and then the rear frame is lifted to continue to move forward. After the rear space is able to accommodate the rear half of the frame, the rear frame falls down. If you want to go to the other side of the pipeline relative to B, rotate in place at B.

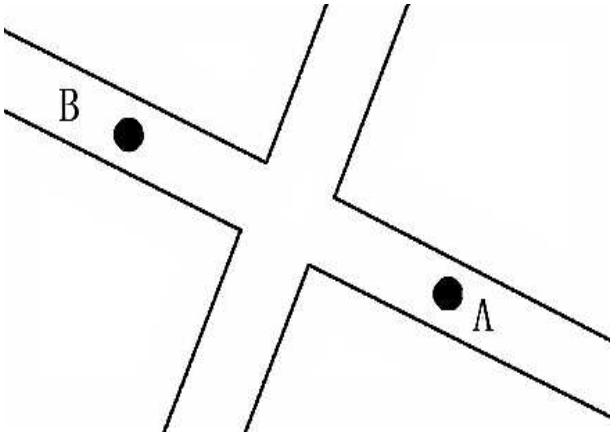

Fig. 10 *schematic diagram of a cross-shaped pipeline parallel to the ground*

5 Motion Simulation Analysis

5.1 Model Assumptions and Virtual Prototype Establishment

The motion form and motion process of the external climbing robot on pipes are quite complicated. Due to the interaction forces among its internal components, it is impossible to establish a flexible system model for the external climbing robot on pipes. However, its overall motion simulation is not significantly affected. Therefore, the following assumptions will be adopted in the analysis below: (a) Assuming that the external climbing robot on pipes only needs to calculate the contact friction force with the pipe wall during its motion, and all of its components are rigid bodies with evenly distributed masses. (b) The direction of the clamping mechanism is at the center axis of the entire device. The ADAMS virtual prototype model of the external climbing robot on pipes is shown in Figure 11.

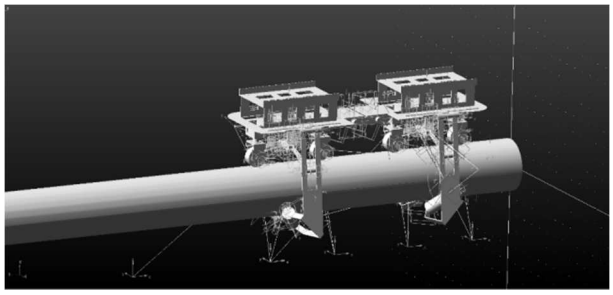

Fig. 11 *Virtual prototype model of pipe climbing robot outside the pipe*

As shown in Figure 11, after importing the crawling robot and the pipeline into ADAMS, in order to facilitate the acquisition of the force conditions during the motion of the crawling robot, contact and motion pair constraints were added between the support wheels, drive wheels, clamping mechanism, rotational joints, and the pipeline. The blue lines in the figure represent the types of motion pairs, the red lines represent collisions between components, and the white lines represent associations with the coordinate system.

5.2 Setting Constraints for Pipe Climbing Robot Contact and Material

Adding fixed pairs between the pipeline and the earth, rotating pairs between the vehicle frame and two clamping arms, flipping mechanism and two vehicle frames, spreader frame and connecting rod, connecting rod and clamping arm, steering drive wheel and clamping arm, and rotating pairs between walking wheels and walking wheel connecting brackets, and mobile pairs between the electric screw and spreader frame. To make it more similar to the real working conditions, contacts need to be added between the various parts of the pipe climbing robot to prevent penetration phenomena during the simulation process, and the added contacts are contacts between entities with friction. In ADAMS, determining the materials, Poisson's ratio, and elastic modulus of each part are crucial for the subsequent motion simulation to proceed, and the material table is shown in Table 1.

Tab. 1 *Material Parameter*

Material	Poisson's ratio	modulus of elasticity(GPa)	density（$10^{-6} kg / mm^3$）
Aluminium alloy	0.33	69	2.74
Rubber	0.47	7.84	1.5

5.3 Simulation of Cross-Vertical Joint Actions with Ground

After pre-processing the virtual prototype model, simulation is carried out for the cross-vertical joint actions. This action combines various actions of the external climbing robot and is simulated due to its requirements for higher load-bearing and adhesion capabilities of the external climbing robot as it climbs up the vertical pipeline. In order to more accurately discover various problems of each action and observe relevant parameter changes more intuitively, the entire action of crossing the vertical and ground joints is decomposed and analysed.The horizontal pipeline motion is analysed. The motor's driving function is set as shown in Table 2.

Tab. 2 *Motor drive function*

Front frame electric screw drive motor	$step(time,0,0,1,-0.5)$
Front frame left turn drive wheel drive motor	$step(time,1,0,2,100)+step(time,4,0,5,-100)$
Front frame right turn drive wheel drive motor	$step(time,1,0,2,-100)+step(time,4,0,5,100)$
Rear frame electric screw drive motor	$step(time,0,0,1,1)$
Rear frame left turn drive wheel drive motor	$step(time,1,0,2,100)+step(time,4,0,5,-100)$
Rear frame right turn drive wheel drive motor	$step(time,1,0,2,-100)+step(time,4,0,5,100)$

After simulation, the following can be obtained for the motion of the external crawler robot in a horizontal pipeline: the torque diagram of the electric screw belonging to the front frame as shown in Figure 12, the torque diagram of the steering drive wheel belonging to the front frame as shown in Figure 13, the curve of the contact force between the steering drive wheel belonging to the front frame and the pipeline as shown in Figure 14, and the displacement change curve of the external crawler robot in the x, y, and z axis as shown in Figure 15. The velocity change curve of the external crawler robot in the x, y, and z axis can be seen in Figure 16.

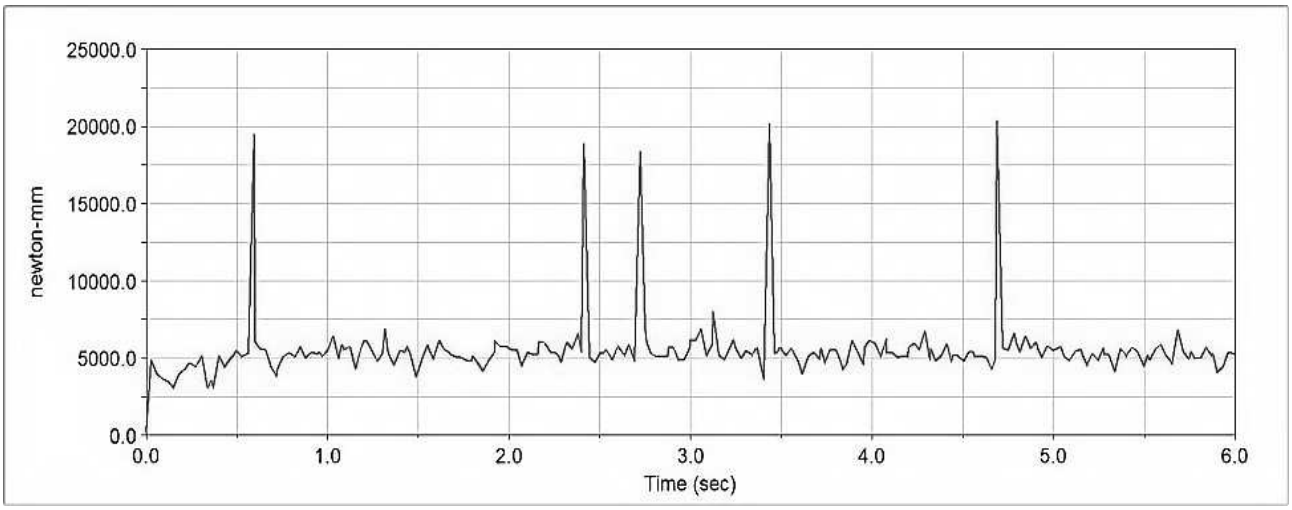

Fig. 12 *Torque diagram of electric lead screw of front frame*

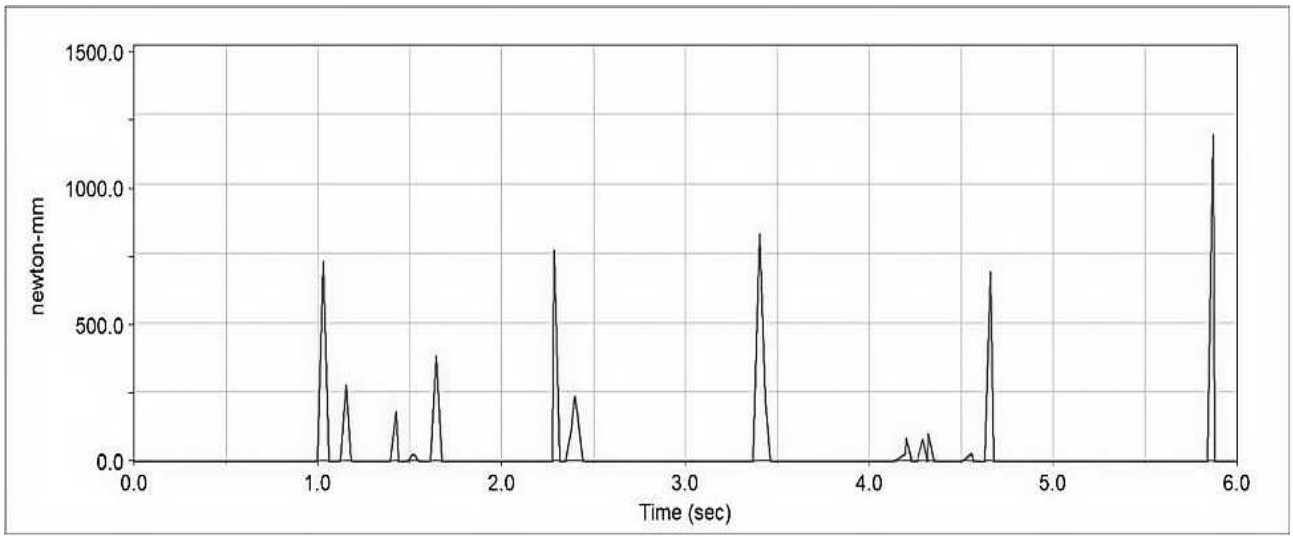

Fig. 13 *Torque diagram of steering drive wheel of front frame*

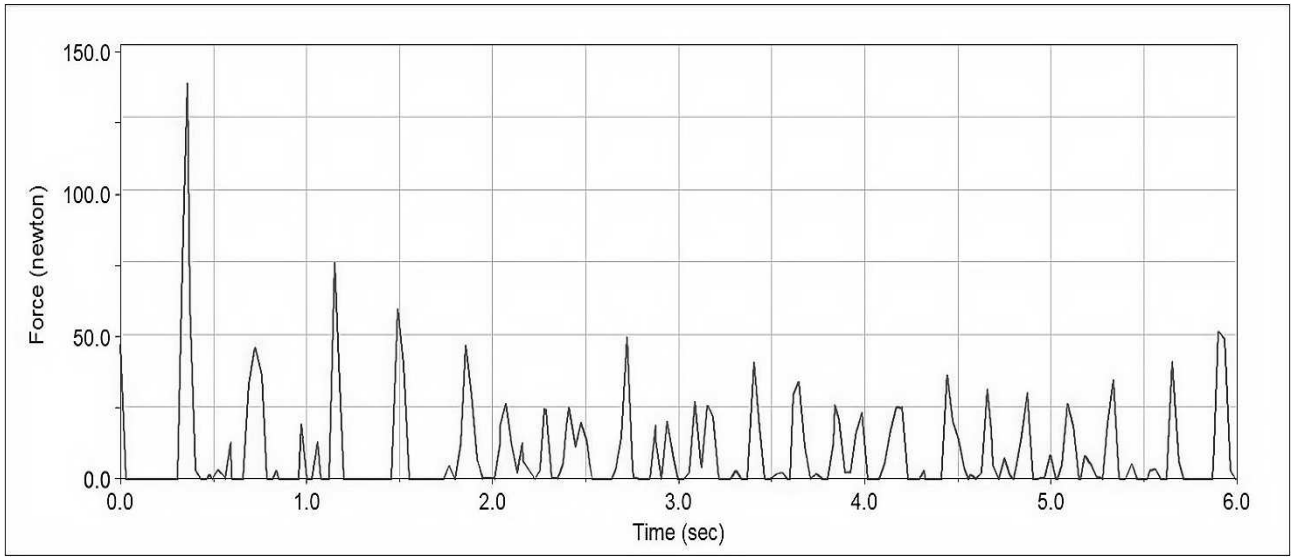

Fig. 14 *Curve of contact force between steering drive wheel of front frame and pipeline*

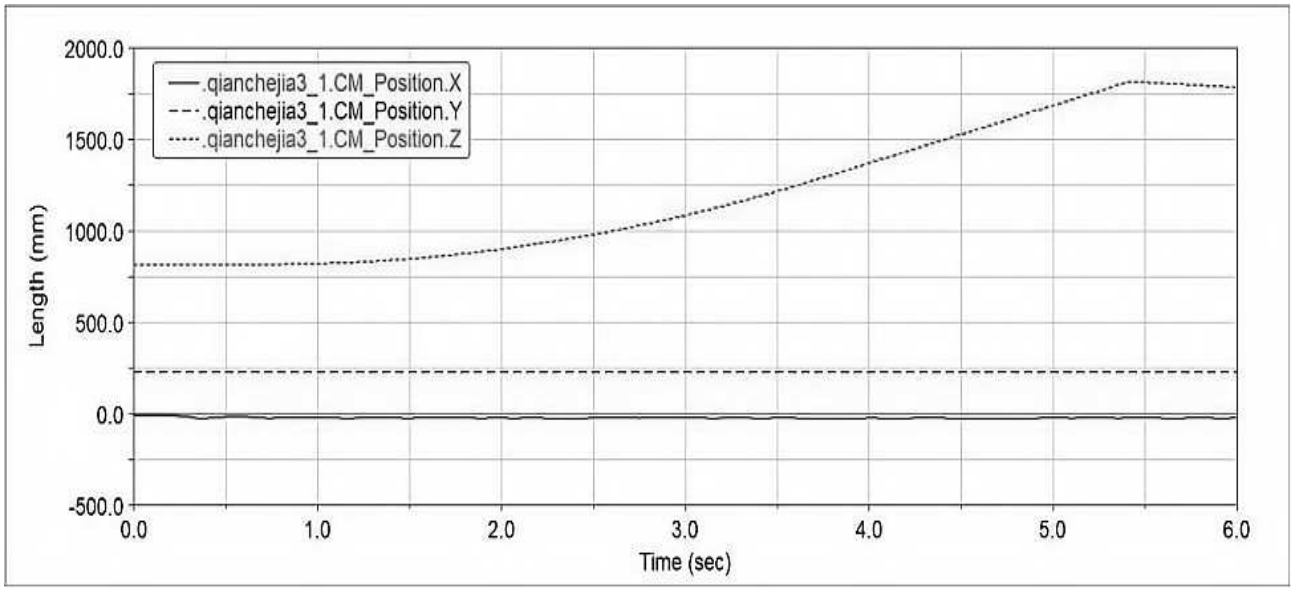

Fig. 15 *displacement curves of the pipe-climbing robot outside the pipe in x, y and z axes*

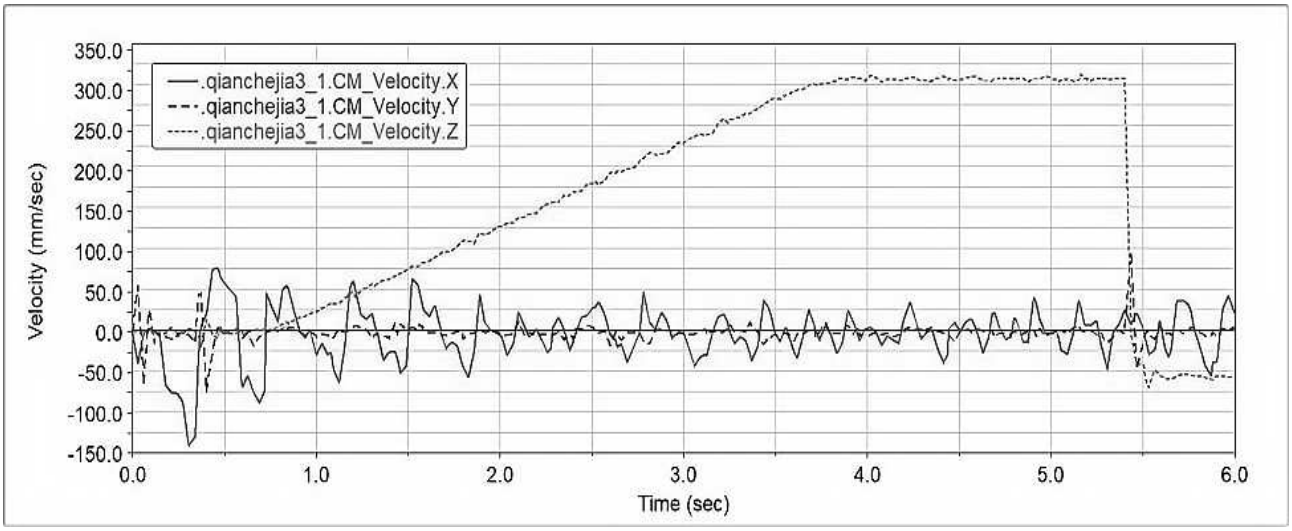

Fig. 16 *velocity variation curves of the pipe-climbing robot outside the pipe in x, y and z axes*

From the torque diagram of the electric screw and the torque diagram of the steering driving wheel, it can be seen that during the movement process, the electric screw is adjusted at all times and can always keep the pipe clamped, but not exceeding the maximum. Therefore, the selection of the electric screw needs to be slightly higher. It can be seen that there is some fluctuation in speed, and the speed reaches the preset 0.3m/s, which can meet the design requirements. The analysis of the flipping mechanism of the robot when working shows that during the forward process, the servo is started and flipped 90 degrees, and the front frame body connected to it is lifted by 90 degrees. The driving function of the motor is shown in Table 3.

Tab. 3 *Expression of Motor Drive Function*

Motor name	Driving function expression
Front frame electric lead screw drive motor	$step(time,0,0,1,-1)$
Flipping mechanism servo motor	$step(time,0,0,2,90d)$
Rear frame electric lead screw drive motor	$step(time,0,0,1,1.5)$
Rear frame left steering drive wheel drive motor	$step(time,0,0,0.5,100)+step(time,1.5,0,2,-100)$
Rear frame right steering drive wheel drive motor	$step(time,0,0,0.5,-100)+step(time,1.5,0,2,100)$

After simulation, the servo torque graph, as shown in figure 17, and the contact force change curve of the steering drive wheel belonging to the rear frame and the pipeline, as shown in figure 18, can be obtained.

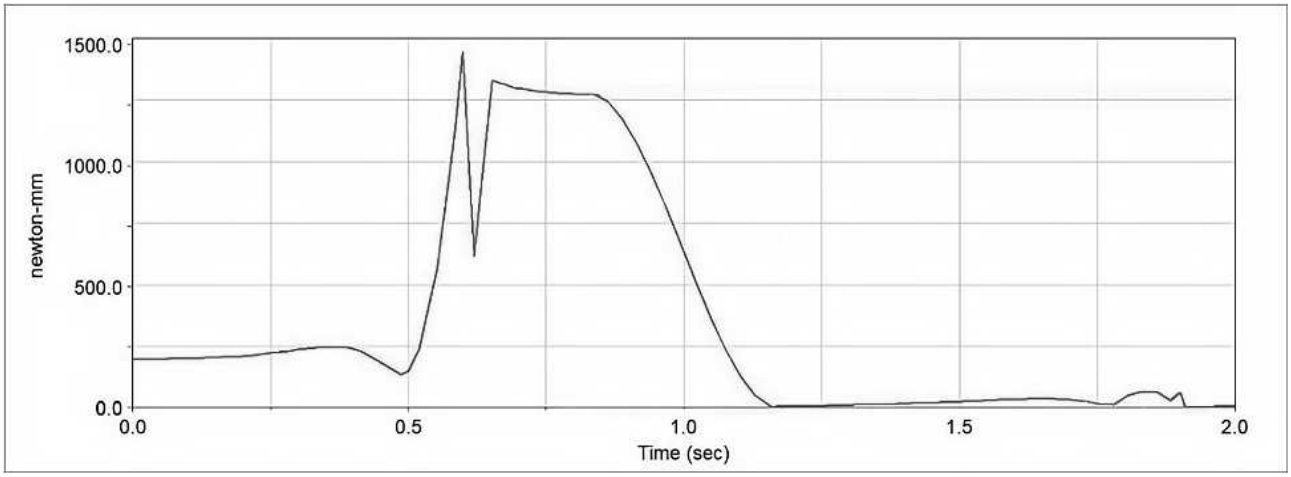

Fig. 17 *Torque variation curve of steering gear*

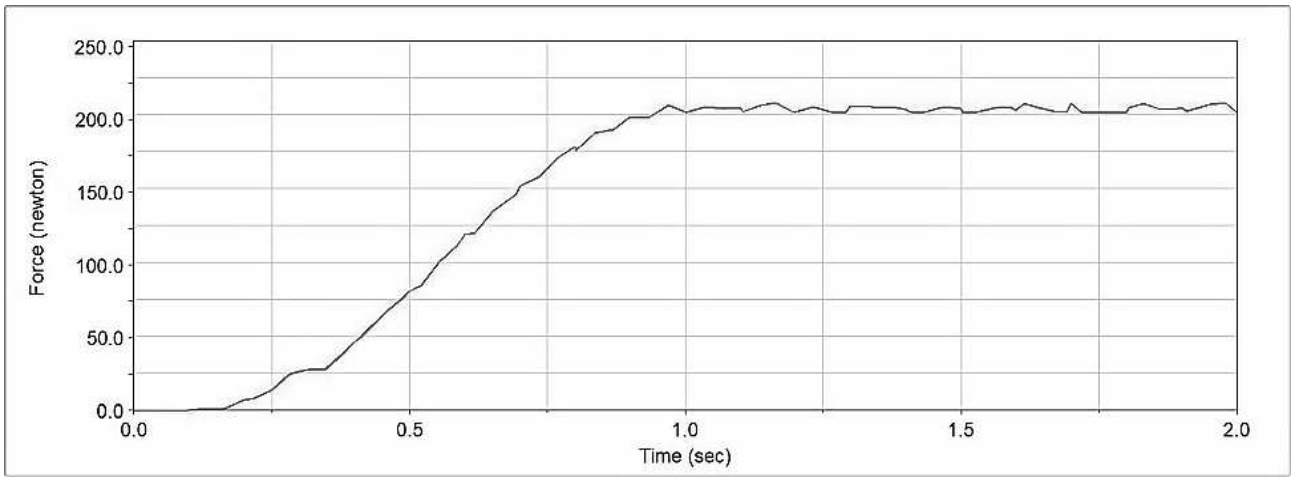

Fig. 18 *Change curve of contact force between steering drive wheel of rear frame and pipeline*

From the torque change chart of the servo, it can be seen that there is fluctuation in the servo torque chart of the flipping mechanism. This is due to the collision vibration caused by the rear turning driving wheel of the external climbing robot and the pipe when the front of the external climbing robot is lifted. The graph of the contact force change between the rear frame steering drive wheel and the pipe indicates that as the servo works, the load borne by the rear frame becomes heavier, so the contact force between the steering drive wheel and the pipe increases. When it reaches the maximum value, the 90-degree flipping action of the servo is completed. Next, the external climbing robot moves forward in a simulation while maintaining the front lift on a vertical pipe, and the motor driving function is shown in Table 4.

Tab. 4 *Motor Drive Function*

Motor name	Driving function expression
The front electric screw-driven motor	$step(time,0,0,1,-0.5)$
a servo motor of the flip mechanism	$step(time,0,0,2,90d)$
an electric screw-driven motor of back frame	$step(time,0,0,1,2)$
a left-turning driving wheel-driven motor	$step(time,1,0,2,100)+step(time,4,0,5,-100)$
a right-turning driving wheel-driven motor	$step(time,1,0,2,-100)+step(time,4,0,5,100)$

After simulation, the variation curves of the contact force between the rear frame body's steering drive wheel and the pipeline can be obtained, as shown in Figure 19. The speed variation curves in x, y, and z axes of the crawler robot outside the pipe are presented in Figure 20, while the displacement variation curves in x, y, and z axes of the crawler robot outside the pipe are shown in Figure 21.

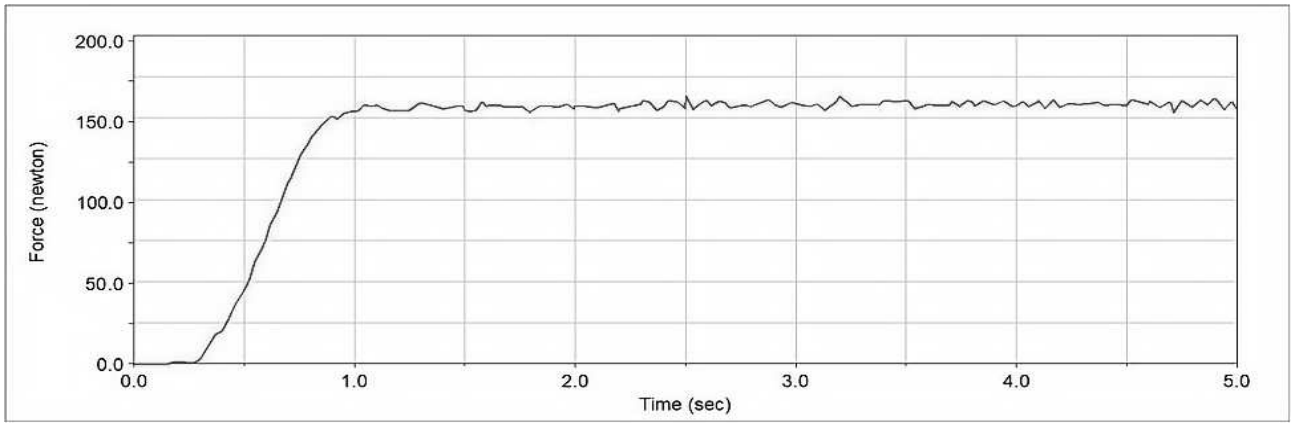

Fig. 19 *Variation diagram of contact force curve between steering drive wheel and pipeline of rear frame body*

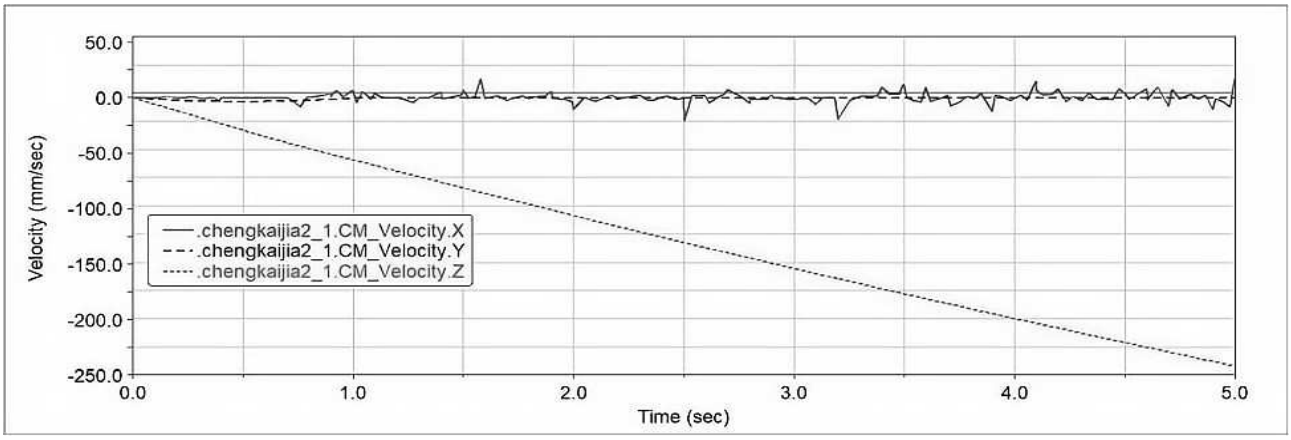

Fig. 20 *velocity variation curves of the pipe-climbing robot outside the pipe in X, Y and Z axes*

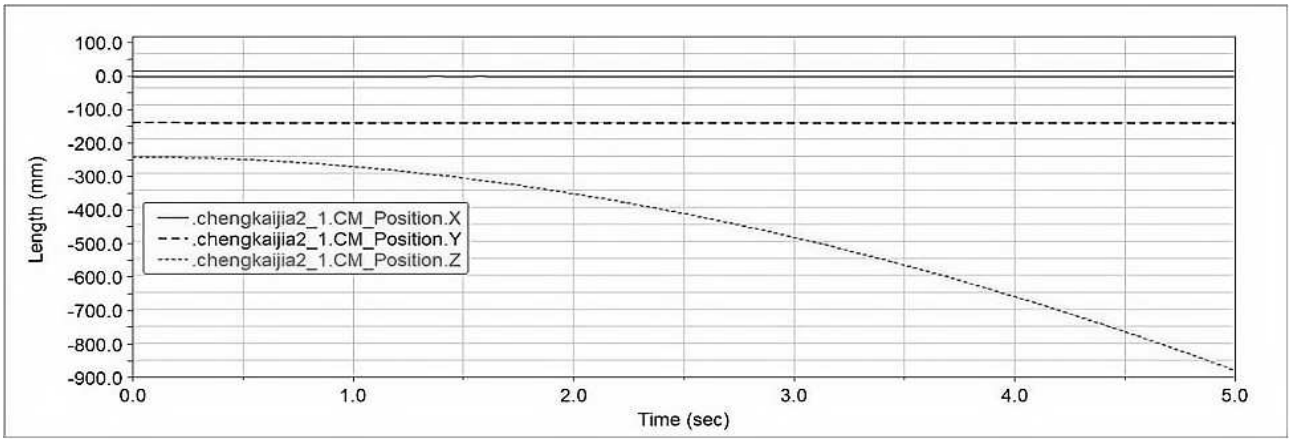

Fig. 21 *displacement change curves of the pipe-climbing robot outside the pipe in X, Y and Z axes*

From the change graph of the contact force curve between the turning and driving wheels and the pipe, it can be seen that the motion of the external climbing robot on the vertical pipe is relatively stable and can pass smoothly. From the speed and displacement change curve of the robot on the x, y, and z axes, it can be seen that the speed and displacement of the external climbing robot is stably increasing, and there is no phenomenon of left and right swing, indicating that the clamping mechanism is working properly and the structural design is reasonable. This proves that the working process of the external climbing robot conforms to the design plan and meets the expected design requirements.

5.4 Simulation of Rotational Motion

After the virtual prototype model, the simulation of the rotating motion is carried out. The specific simulation analysis process is as follows: (a) The external climbing robot's clamping mechanism clamps the pipe and adjusts its own position to be parallel to the pipe. (b) The turning and driving wheels belonging to the front chassis body, and the robot rotates to the left. The driving function of the motor is set as shown in Table 5.

Tab. 5 *Motor Drive Function*

Motor name	Driving function expression
Front frame body electric push rod drive motor	$step(time, 0, 0, 0.5, 1)$
Front frame body left steering drive wheel drive motor	$step(time, 0.5, 0, 2, -100)$
Front frame body right steering drive wheel drive motor	$step(time, 0.5, 0, 2, -100)$
Rear frame body electric push rod drive motor	$step(time, 0, 0, 0.5, 1)$
Rear frame body left steering drive wheel drive motor	$step(time, 0.5, 0, 2, -100)$
Rear frame body right steering drive wheel drive motor	$step(time, 0.5, 0, 2, -100)$

After simulation, the force curve of the walking wheel belonging to the rear chassis body in contact with the pipeline during the rotation process can be obtained for the climbing robot outside the pipe, as shown in Figure 22, the velocity change curve of the walking wheel belonging to the rear chassis body, as shown in Figure 23.

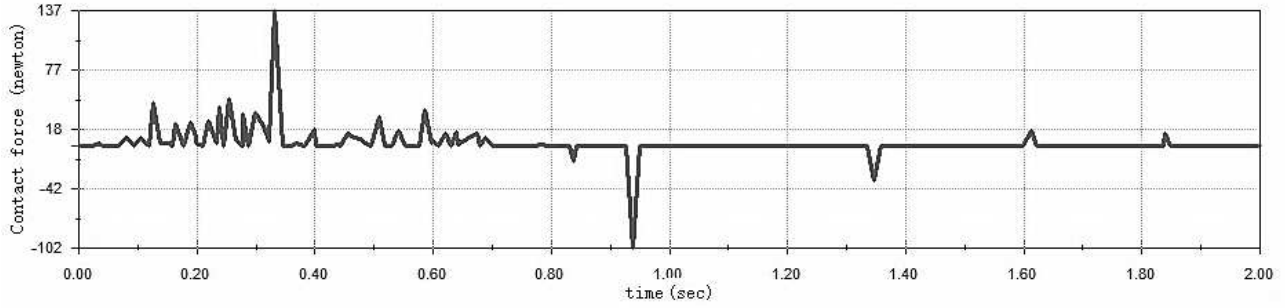

Fig. 22 *Curve of contact force between walking wheel and pipeline of rear frame body*

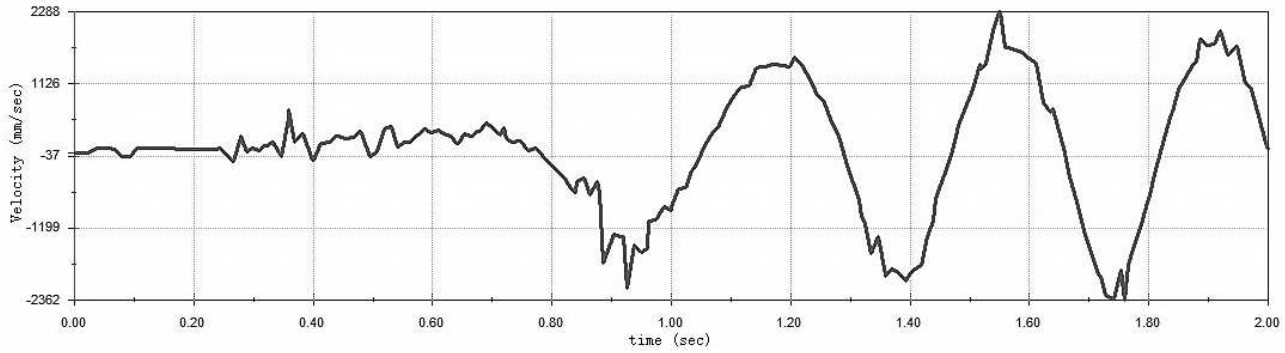

Fig. 23 *Curve of speed change of walking wheels of rear frame body*

The contact force curve of the walking wheel and pipeline indicates the existence of vibration in the external climbing robot. This is due to the vibration generated by the friction between the walking wheel and the pipeline during the movement of the external climbing robot. As shown by the velocity change curve, after experiencing the initial smooth speed, the velocity changes become regular. The motion status of the external climbing robot is slowly rotating upwards, then rotating downwards under gravity, completing a rotational motion by relying on inertia, and the slight changes in velocity are also due to vibration. The overall motion conforms to the design.

6 Conclusion

For different external pipe situations, multiple climbing actions are designed, and the vibration stability of the robot's external climbing is analyzed. It is found that the material has a significant impact on the vibration characteristics of the mechanism. Therefore, aluminum alloy is selected as the main material in the later motion simulation process. Using ADAMS software for kinematic analysis, a virtual prototype model is established to analyze the changes in various parameters of the external climbing robot when rotating around the pipeline and overcoming obstacles, obtaining changes in displacement, velocity, acceleration, contact force, and torque curves, which confirms the feasibility of the robot's motion and provides a basis for the operation of the prototype.

Acknowledgement

The Natural Science Foundation of Shandong Province (No.ZR2020QE151) and Qingdao Huanghai University doctoral research Fund Project (2020boshi02).

References

[1] JAN, K., KRISTINA, B., OLEKSANDR, P., NADIIA, A. (2022). Erosion Modelling of Structural Materials in the Working Space of Multistage Convective Dryers. In: *Manufacturing Technology*, Vol. 22, No.4, pp. 307-318. ISSN 1213-2489.

[2] SHIYUN LI, CHENGHONG XU. (2022).The Impact of Industrial Robots on China's Regional Industrial Structure. In: *Regional Research and Development*, Vol. 41, No. 1, pp.6-12.ISSN1003-0670.

[3] PAVOL, T., TATIANA, C., ANDREJ, C., SILVIA, S., JOZEF, H., MIROSLAV, C. (2022). Analysis of Parameters of Sintered Metal Components Created by ADAM and

SLM Technologies. In: *Manufacturing Technology*, Vol. 22, No. 4, pp. 347-355. ISSN 1213-2489.

[4] AIHUA SHEN. (2022). Industrial Robot - Key Equipment for Automation.In: *Rubber Technology and Equipment*, Vol. 48, No.02, pp.58-65. ISSN 1009-797X.

[5] ZHIHONG YANG, JIANWU YU, JUXIN WANG, et al. (2021).Lightweight Design and Dynamic Performance Analysis of Cable Detection Climbing Device. In: *Machinery Design and Manufacturing*, Vol. 21, No. 10, pp. 57-61.ISSN 1001-3997.

[6] LIAO Y. Y., LIAO B. Y. (2021).Lightweight Design and Optimization Effect Evaluation of Hydro Generator Set. In: *Manufacturing Technology*, Vol. 21, No.2, pp. 223-230.ISSN 1213-2489.

[7] TUONG N. V., NAPRSTKOVA, N. (2019). Matlab-based Calculation Method for Partitioning a Free-form Surface into Regions. In: *Manufacturing Technology*, Vol. 19, No.3, pp. 518-524.ISSN 1213-2489.

[8] DING MAO, GENG DA, ZHOU MINGDONG, et al. (2021). Structural strength topology optimization strategy based on variable density method.In: *Journal of Shanghai Jiaotong University*, Vol. 55 No.6, pp.764-773.ISSN 1006-2467.

[9] LUBIN WANG, FULIN HE, YAJUAN HE, et al. (2020). Simulation research on torsional stiffness of plastic tailgate based on finite element analysis.In: *Manufacturing Automation*, Vol.42, No.11, pp.129-132.ISSN 1009-0134.

[10] CHAO CHEN, HEHE CHEN, SHUTING WU, et al. (2021). Structural optimization of industrial robot manipulator. In: *Machine Tool and Hydraulic*, Vol.49, No03, pp.25-29.ISSN 1001-3881.

[11] JIANCHAO HE, FENG QIAN, XIANGYUAN LI, et al. (2022). Dynamic simulation analysis of multi-link mechanism with clearance.In: *Electromechanical Engineering Technology*, Vol.51, No.01, pp.42-45.ISSN 1009-9492.

[12] JIANMIN HUANG, JUN ZHONG, DECHEN XIA. (2021).Research on design system of multi-link press rod based on MATLAB.In: *Forging Equipment and Manufacturing Technology*, Vol.56, No.06, pp.13-18.ISSN 1000-3940.

[13] HAOHAO MA, YANWEI FENG, BAOZHEN YAO. (2021).Dynamic simulation analysis of slider crank fixed type mechanism based on ADAMS.In: *Mechanical Research and Application*, Vol.34, No.06, pp.19-21.ISSN 1007-4414.

[14] XU, W., PAN, E., LIU, J., LI, Y., YUAN, H. (2021). Flight control of a large-scale flapping-wing flying robotic bird: system development and flight experiment. In: *Chinese Journal of Aeronautics*, Vol. 35, No. 2, pp. 235-249. ISSN 1000-9361.

[15] TETSUSHI K., TAICHI A., SATOSHI S. (2020). Development of a separable search-and-rescue robot composed of a mobile robot and a snake robot. In: Advanced Robotics, Vol. 34, No. 2, pp. 132-139. ISSN 0169-1864.

[16] GOUGH, E., CONN, A., ROSSITER, J. (2021). Planning for a tight squeeze: navigation of morphing soft robots in congested environments. In: *IEEE Robotics and Automation Letters*, Vol. 6, No. 3, pp. 4752-4757. ISSN 2377-3766.